



Differential attraction and repulsion of *Staphylococcus aureus* and *Pseudomonas aeruginosa* on molecularly smooth titanium films

SUBJECT AREAS:
NANOBIOTECHNOLOGY
CELLULAR MICROBIOLOGY
BIOPHYSICS
CELL BIOLOGY

Received
27 July 2011

Accepted
27 October 2011

Published
22 November 2011

Correspondence and
requests for materials
should be addressed to
E.P.I. (eivanova@swin.
edu.au)

Elena P. Ivanova¹, Vi Khanh Truong¹, Hayden K. Webb¹, Vladimir A. Baulin^{2,3}, James Y. Wang⁴, Narges Mohammadi¹, Feng Wang¹, Christopher Fluke⁵ & Russell J. Crawford¹

¹Faculty of Life and Social Sciences, Swinburne University of Technology, PO Box 218, Hawthorn, Victoria, 3122, Australia, ²ICREA, 23 Passeig Lluís Companys, 08010 Barcelona, Spain, ³Departament d'Enginyeria Química, Universitat Rovira i Virgili 26 Avenue dels Paisos Catalans, 43007 Tarragona, Spain, ⁴Faculty of Engineering and Industrial Sciences, IRIS, Swinburne University of Technology, PO Box 218, Hawthorn, Victoria, 3122, Australia, ⁵Centre for Astrophysics and Supercomputing Swinburne University of Technology, PO BOX 218, Hawthorn, Victoria, 3122, Australia.

Magnetron sputtering techniques were used to prepare molecularly smooth titanium thin films possessing an average roughness between 0.18 nm and 0.52 nm over 5 $\mu\text{m} \times 5 \mu\text{m}$ AFM scanning areas. Films with an average roughness of 0.52 nm or lower were found to restrict the extent of *P. aeruginosa* cell attachment, with less than 0.5% of all available cells being retained on the surface. The attachment of *S. aureus* cells was also limited on films with an average surface roughness of 0.52 nm, however they exhibited a remarkable propensity for attachment on the nano-smoother 0.18 nm average surface roughness films, with the attachment density being almost twice as great as that observed on the nano-rougher film. The difference in attachment behaviour can be attributed to the difference in morphology of the rod-shaped *P. aeruginosa* compared to the spherical *S. aureus* cells.

Since the advent of micro/nano-fabrication, bacterial interactions with material surfaces have been the focus of a number of intensive research programs^{1–5}. It has become clear that surface micro/nano-topography plays a critical role in bacterial attachment^{6–13}. A number of different approaches have been adopted to investigate the bacterial response to surfaces containing different topographies, including those fabricated with regular patterns or native irregular material topographies^{1,7–8,14–21}. For example, *P. aeruginosa* and *S. aureus* cells were found to attach to surfaces containing regularly spaced pits of 1 μm and 2 μm in size, yet not to surfaces containing irregularly spaced pits of 0.2 μm and 0.5 μm in size¹⁶. Díaz *et al.* reported that *E. coli* cells were able to successfully attach and align on surfaces containing microgrooves of 1.3 μm width and 120 nm depth¹⁴, yet unable to attach and align on surfaces with the groove height of 50 nm and period of 1.6 μm ¹. Mitik-Dineva *et al.* found that the presence of pits of 2.5 μm diameter on the surfaces of etched optical fibers restricted the extent of bacterial attachment compared to that obtained on unmodified optical fiber surfaces, which contain irregular topographies with an average height of 181 nm¹³. Several studies have shown that bacterial attachment is modulated by the presence of regular submicron- and micron-scale surface topographies when the dimension of these topographies is greater than about 100 nm^{7–8,14,16}. Rowan *et al.* fabricated arrays of regular micron-scale patterns of size 83 μm and 12 μm on polyethylene glycol surfaces and were able to localize *E. coli* cells on these surfaces⁷. Rozhok *et al.* fabricated 3 μm diameter holes of 0.5 μm depth in which single *E. coli* cells were successfully localized⁸. In addition, several studies have utilized not only surface micron-scale topography but also the surface chemistry of the substrate to control the extent of bacterial attachment. For example, Rowan *et al.* and Rozhok *et al.* used poly(ethylene glycol) and poly-L-lysine substrates (respectively) to enhance the degree of bacterial attachment^{7–8}. The influence of the surface nanotopography of glass and metal oxide substrates (with an average roughness R_a of 4.1 to 17.6 nm) on bacterial attachment was reported by Li and Logan²⁰. It was found that both surface chemistry and topography influenced the extent of bacterial attachment, but no conclusions were drawn regarding the relative influences of these surface characteristics on the extent of bacterial attachment. Bacterial interactions with metallic surfaces of various surface topographies has also received significant attention



over the last few decades^{16–19,21}. However, there is no consensus regarding whether increased levels of surface roughness can be correlated either positively or negatively to the extent of bacterial attachment, often as a result of inconsistent results and a lack of systematic studies being performed^{16–19,21}. For instance, one study reported that *S. epidermidis* cells were not able to effectively attach onto titanium surfaces with an average surface roughness between 1.25 μm and 0.43 μm ¹⁷. Another study reported that no significant bacterial attachment was found on stainless steel surfaces with an average roughness varying from 1.04 μm to 0.01 μm ¹⁸. A subsequent study, however, reported that only minimal bacterial attachment was observed on metallic surfaces with an average roughness of 0.6 μm , whereas surfaces either smoother or rougher than these allowed a greater number of bacterial cells to attach¹⁹. Whitehead *et al.* studied bacterial attachment on titanium dioxide surfaces with different degrees of nano-scale roughness²¹. This work highlighted that *S. aureus* cells were able to attach in greater number to surfaces exhibiting an average roughness of 8.7 nm than that observed for surfaces of average roughness of 43.6 nm, yet *P. aeruginosa* cells were found to behave in the opposite way²¹. A few recent studies have shown that bacterial cells were able to attach more efficiently onto titanium surfaces containing an average surface roughness of below 1.2 nm^{22–23}. A similar increased level of attachment was also reported for glass surfaces possessing an average roughness of 1.3 nm than those for an average surface roughness of 2.1 nm^{12,15}.

Despite the growing body of evidence indicating that the extent of bacterial cell attachment is enhanced on surfaces containing nanometric scale roughness^{2,9–10,12–13,15,22–23} and that bacterial cells appear to be able to detect a change in the average surface roughness down to dimensions as low as 1 nm, it remains unclear as to whether molecularly smooth surfaces containing surface roughness on the sub-nanometric scale represent a boundary below which the surface nanotopography restricts the extent of bacterial attachment. There appears to be a paucity of work reporting the extent of bacterial attachment on sub-nanometrically smooth surfaces, and the influence (if any) of this surface architecture on the attachment process. This paper was designed as an extension of our previous work^{2,12–13,15,22–23} to fill this gap in the existing knowledge. We employed a magnetron sputtering technique for fabricating the titanium thin films^{24–25}. This approach allowed the controlled atomic deposition of titanium onto a substrate for the purposes of producing metallic thin films with sub-nanoscale and nanoscopic surface roughness^{24–25}. Titanium thin films with an average surface roughness of 0.5 nm, 0.2 nm, and 0.18 nm with corresponding film thickness of 150 nm, 12 nm, and 3 nm, respectively, were fabricated on silicon wafers with an initial average surface roughness of 0.29 nm. We have previously shown that the two strains of bacteria, *P. aeruginosa* and *S. aureus*, have the ability to differentiate between surfaces exhibiting very small differences in surface roughness, with a reduction in the average surface roughness from 1.22 nm to 0.58 nm resulting in a 2 to 3-fold increase in the number of attached cells, together with an elevated level of extracellular polymeric substances secretion on the surface. The aim of this study was to investigate the extent of bacterial attachment on the molecularly smooth (i.e. sub-nanometric roughness) titanium thin film surfaces in an attempt to locate the boundary, if any, of surface roughness that is able to influence the extent of bacterial attachment on surfaces.

Results

Physicochemical Characterization of Titanium Surfaces. The surfaces of the titanium thin films were found to be hydrophobic, displaying water contact angles between 96° and 104.5° (Supporting Information: Table S1). It appeared that the surface hydrophobicity increased with increased film thickness (statistically significant; *t*-test: *t* = 0.03 (*p* < 0.05)), with measured contact angles being approximately 96°–97° for the 3 nm and 12 nm films and 104.5°

for the 150 nm films. The surface free energies were found to be low (due to the high proportion of the dispersive components), ranging from 36 mN m⁻¹ for the 3 nm and 12 nm films to 39.5 mN m⁻¹ for the 150 nm films.

An XPS analysis confirmed that the surfaces of the 12 nm and 150 nm titanium films were homogeneously covered by titanium with a concentration increasing from 17.7 at% in the 3 nm films to 21.7 at% in the 150 nm films. Up to 8.5 at% of silicon was detected on the 3 nm thickness films, due to the depth of XPS analysis being nominally around 3–5 nm. Overall, titanium and oxygen were found to be the most abundant elements on the surface of the films. The high resolution XPS spectra of titanium displayed three peaks, in which the binding energy peaks at ~458.0 eV and ~463 eV for titanium surfaces are attributable to TiO₂, confirming the previously reported similar observations^{22,26–28}.

The singlet ground electronic state (X1A¹) of the TiO₂ molecule possesses a C_{2v} point group symmetry, which is given in Fig. 1. The geometric and electronic properties of TiO₂ are given in Table 1. TiO₂ has two equal Ti–O bond lengths of 1.641 Å with an O–Ti–O angle of 111.9°, providing good agreement between theory and experiment. For example, the B3LYP/LANL2DZ model produces the Ti–O bond length and O–Ti–O bond angle as 1.685 Å and 110.8°²⁹, respectively, and the CCSD(T)/LANL2DZ model reported as 1.672 Å and 112.6°²⁹, respectively. Experimentally, only an estimate exists of the O–Ti–O angle (110 ± 5°) for the singlet ground electronic state. The electronic spatial extent <R²> reaches 193.95 au, which corresponds to approximately 10 nm; the molecular electrostatic potential (MEP) is shown in Fig. 1.

Titanium Thin Film Surface Topography and Morphology. The results of an AFM surface roughness analysis of the silicon wafer and the 3 nm, 12 nm and 150 nm titanium thin films over two scanning areas, 10 μm × 10 μm and 5 μm × 5 μm , are shown in Table 2 and Fig. 2. Five parameters were used for the characterization of the

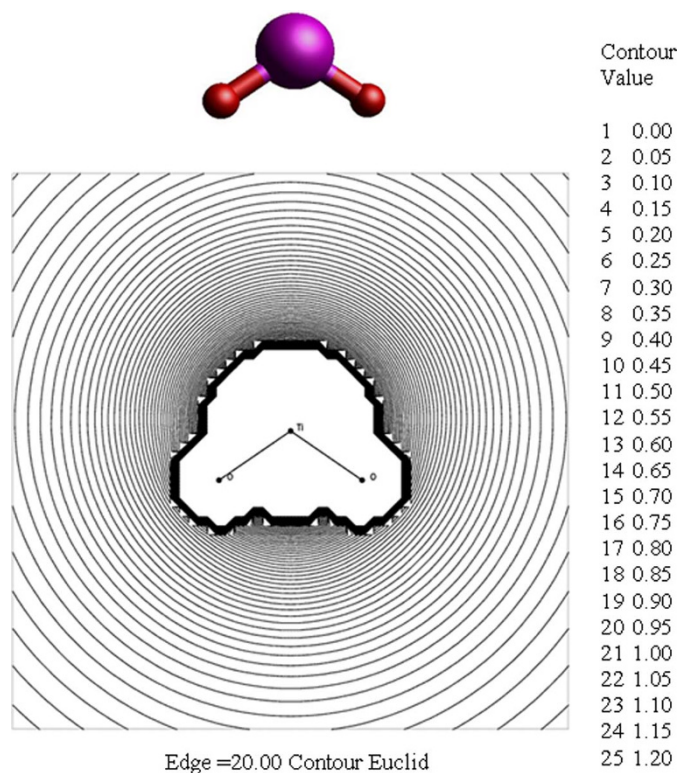


Figure 1 | The optimized geometry of TiO₂ (top) and molecular electrostatic potential (MEP) of TiO₂ using B3LYP/cc-pVTZ model (bottom).

Table 1 | Comparison of properties of TiO₂ in its singlet ground electronic state (X1A¹).

Properties	This work	Ref ^a	Ref ^b
	B3LYP/cc-pVTZ	B3LYP/LANL2DZ	Experiment
R _{Ti-O} (Å)	1.641	1.658 (1.672) ^d	NA
O-Ti-O (°)	111.9	110.8 (112.6) ^d	110 ± 5
E _{A_g} (eV)	1.61	1.69	1.59 ± 0.03
IP _a (eV)	9.62 ^c	9.75	9.5 ± 0.1
<R ² > (au)	193.95		
μ (Debye)	6.65		
Rotational Constants (GHz)	a: 31.23505 b: 8.54663 c: 6.71049		

^aData obtained from²⁹.
^bData obtained from³⁰.
^cIP is calculated as E_{cation} - E_{neutral}.
^dThe CCSD/LANL2DZ values in parentheses.

surfaces: average roughness (R_a), root mean square (RMS) roughness (R_q), maximum height (R_{max}), skewness (R_{skw}) and kurtosis (R_{kur})^{22,31–32}. Three parameters including R_a , R_q and R_{max} were utilized to evaluate the titanium thin films' surface topography, while skewness and kurtosis were used to describe the surface morphology. The surface topography of the 3 nm and 12 nm films appeared to be similar and remarkably smooth on the sub-nanometer scale, i.e., R_a of 0.18 nm and 0.20 nm and R_q of 0.20 nm and 0.24 nm on the 10 μm × 10 μm scanning areas; and R_a of 0.19 nm and 0.20 nm and R_q of 0.20 nm and 0.24 nm on the 5 μm × 5 μm scanning areas, respectively (Table 2). The differences between the roughness parameters for the 3 nm and 12 nm titanium thin films on both scanning areas were not statistically significant ($t = 0.24$ for R_a and 0.20 for R_q on 10 μm × 10 μm; $t = 0.19$ for R_a and 0.09 for R_q on 5 μm × 5 μm, $p > 0.05$). The R_a and R_q parameters of the silicon wafer surfaces were in the range 0.27 nm to 0.37 nm on both scanning areas. The surface roughness of the 150 nm thin films remained on the sub-nanometric scale; however, the roughness exhibited was approximately 2–2.5 times greater than that of the uncoated substratum. A statistical analysis of the R_{max} data obtained for the 10 μm × 10 μm and 5 μm × 5 μm scanning areas highlighted that there was no significant difference between the maximum height of the uncoated silicon wafer and the 3 nm, 12 nm and 150 nm titanium films ($p > 0.05$).

As previously reported, skewness is commonly used to describe the symmetry of the surface and kurtosis is used to measure the peakedness of the surface^{22,31–32}. All of the titanium surfaces studied here showed a R_{skw} close to 0 and a R_{kur} close to 3, indicating that the surfaces exhibited a symmetrical distribution of approximately bell-shaped peaks and valleys (Table 2)^{22,31–32}. No statistically significant difference was found to exist between the R_{kur} for the three titanium thin films on both scanning areas ($p > 0.05$), while the R_{skw} appeared to be statistically significantly different only for the 10 μm × 10 μm scanning areas. The R_{skw} and R_{kur} values for the 3 nm and 12 nm films were not statistically significantly different for the 5 μm × 5 μm

scanning area samples ($t = 0.69$ and 0.44 respectively, $p > 0.05$), in contrast to those of the 150 nm films, confirming that the peaks formed on the 150 nm surfaces were higher and sharper and valleys of these surfaces were shallower and broader than the other samples.

***P. aeruginosa* and *S. aureus* interaction with molecularly smooth titanium thin film surfaces.** Analysis of the bacterial retention patterns that were visualized using scanning electron microscopy (SEM) and confocal scanning laser microscopy (CSLM) indicated that the *P. aeruginosa* and *S. aureus* cells responded in different ways to the surface that were smooth on a sub-nanometric scale. The cell densities of *P. aeruginosa* on the titanium film surfaces were found to be low and not statistically significantly different on each of the three film surfaces ($t = 0.84$, $p > 0.05$). While *P. aeruginosa* appeared to be a poor colonizer of the surfaces, *S. aureus* was able to successfully colonize the surfaces of each of the titanium films (Supporting Information: Table S3, Fig. 3–4). The proportion of cells retained on the 3 nm and 12 nm film surfaces, with an R_a of approximately 0.20 nm, was almost equivalent (no statistically significant difference $t = 0.28$, $p > 0.05$) and more than double that obtained on the 150 nm films, with an R_a of approximately 0.52 nm ($t = 0.01$ and 0.04 respectively, $p < 0.05$). Notably, both bacterial strains produced an elevated amount of extracellular polymeric substances (EPS), as inferred from the COMSTAT analysis of the CSLM images, on both the 3 nm and 12 nm films (Fig. 3), but not on the 150 nm films ($t = 0.003$, $p < 0.05$).

Discussion

Silicon wafers that were smooth on the sub-nanometric scale were used as a substratum for titanium thin film deposition, and the evolution of the surface morphology of the resultant films is shown in Fig. 2(II). The change in the surface morphology of the films is due to the shadow effect resulting from the sputtering process³³. As the atomic deposition results in a growing film with the height $h(x,t)$, the explanation of shadow effect was formulated according to³³:

Table 2 | AFM surface roughness analysis of titanium thin film surfaces

	Ti film thickness	Average roughness (nm) R_a	RMS roughness (nm) R_q	Maximum height (nm) R_{max}	Skewness R_{skw}	Kurtosis R_{kur}
10 μm × 10 μm	0 nm	0.27 ± 0.05	0.37 ± 0.04	17.41 ± 3.85	0.03 ± 0.01	3.12 ± 0.06
	3 nm	0.19 ± 0.01	0.22 ± 0.01	2.81 ± 0.17	-0.09 ± 0.01	3.47 ± 0.07
	12 nm	0.20 ± 0.01	0.24 ± 0.01	6.61 ± 1.04	0.11 ± 0.01	2.63 ± 0.51
	150 nm	0.66 ± 0.01	0.83 ± 0.01	7.59 ± 0.35	0.63 ± 0.04	3.79 ± 0.16
5 μm × 5 μm	0 nm	0.29 ± 0.01	0.37 ± 0.02	8.77 ± 1.71	0.37 ± 0.07	5.70 ± 1.40
	3 nm	0.18 ± 0.01	0.20 ± 0.02	3.30 ± 0.17	-0.08 ± 0.01	3.48 ± 0.03
	12 nm	0.20 ± 0.01	0.24 ± 0.01	3.93 ± 0.71	-0.07 ± 0.04	2.86 ± 0.71
	150 nm	0.52 ± 0.01	0.68 ± 0.03	6.00 ± 0.17	0.43 ± 0.10	3.35 ± 0.31

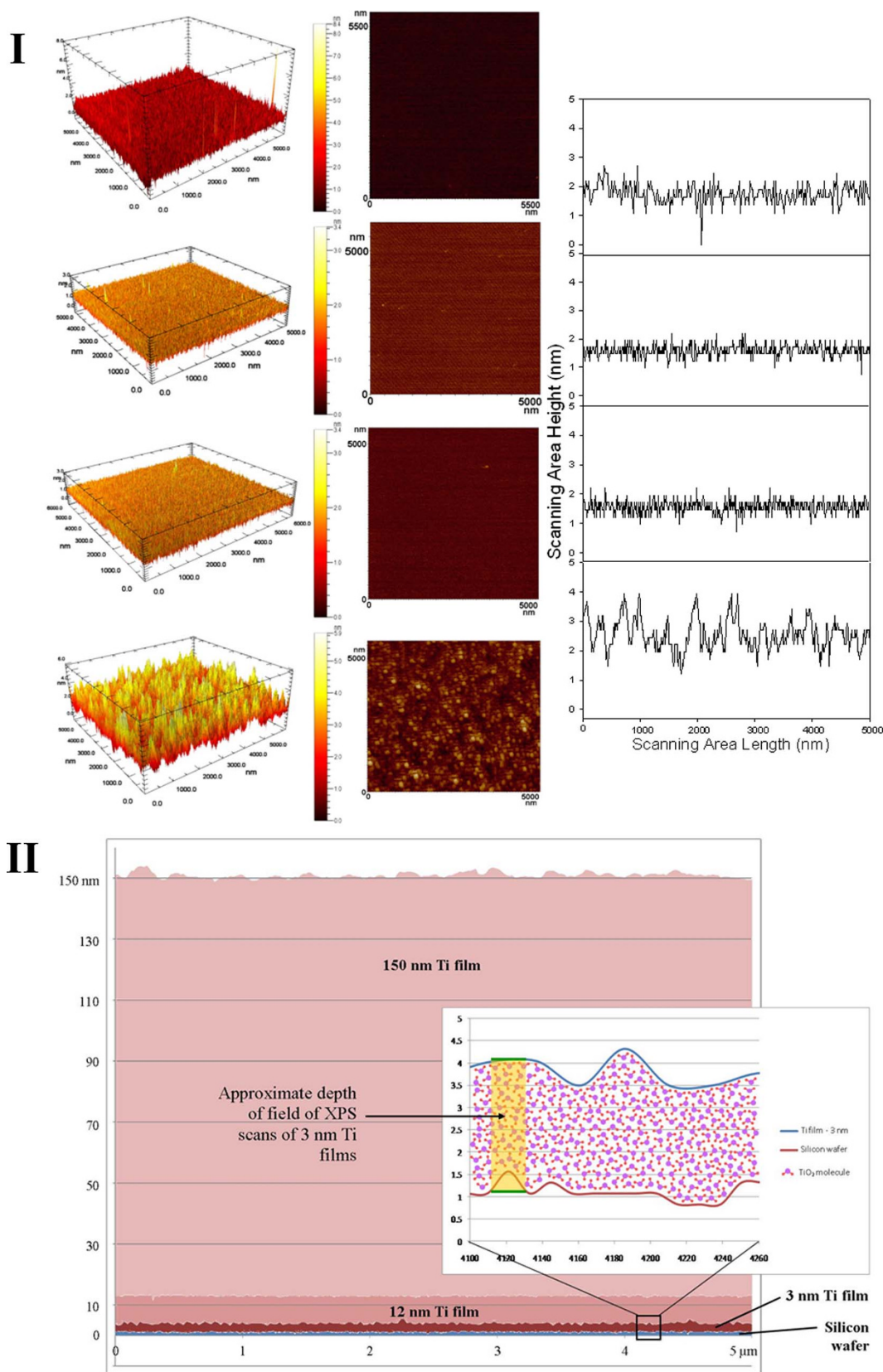


Figure 2 | Typical 3D AFM images and corresponding surface profiles of silicon wafer (a) and titanium thin film (b, c, d respectively for 3 nm, 12 nm and 150 nm Ti thin films) surfaces from approximately $5\ \mu\text{m} \times 5\ \mu\text{m}$ scanned areas (I). Formation of nanograins can be seen on Ti thin films.

Interactive, 3-dimensional views of the data are presented in Supplementary Figure S4: Readers using version 8.0 or higher of Acrobat Reader can enable interactive views by clicking on the figure panels. Once enabled, 3-d mode allows the reader to rotate and zoom the view using the computer mouse.

(II) Evolution of surface roughness after serial-deposition of Ti on silicon wafer. Figure was constructed from typical surface profiles, by plotting on the same set of axes, with the mean line of each profile set to the thickness of its corresponding film. Inset is a schematic approximation of how deposited TiO_2 molecules form a 3 nm thin film. A silicon (8.5 at%) was detected during XPS scans of 3 nm films due to the XPS field-depth, as shown how in certain parts of the film the underlying substrate can be detected.

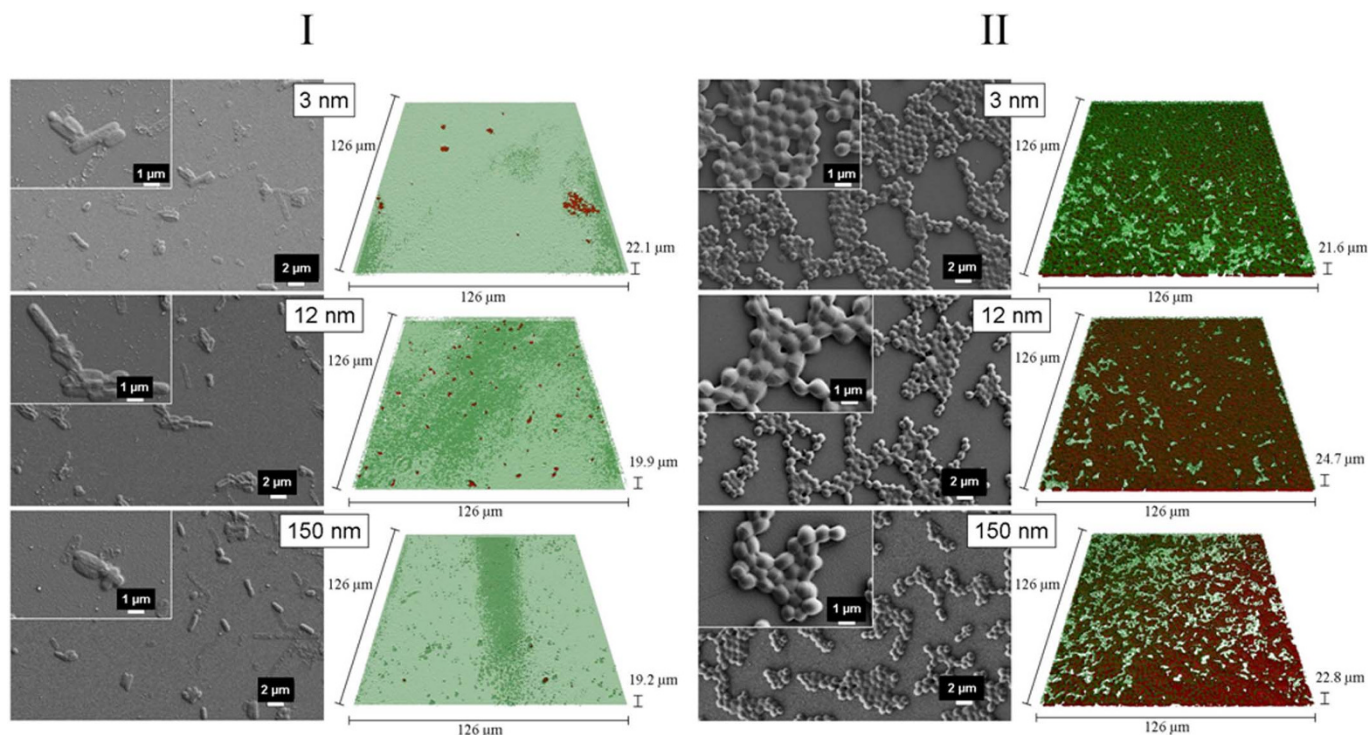


Figure 3 | Typical SEM images (left) of *P. aeruginosa* (I) and *S. aureus* (II) retention patterns onto titanium thin film surfaces of 3 nm (a), 12 nm (b) and 150 nm (c) thicknesses after 18 h incubation. Three-dimensional visualization (projections of CSLM images) (right) of representative *P. aeruginosa* (I) and *S. aureus* (II) specimens on the titanium thin film surfaces of 3 nm (a), 12 nm (b) and 150 nm (c) thicknesses after 18 h incubation and corresponding quantification of viable cells (colored red) retained on the surfaces.

$$\frac{\partial h}{\partial t} = -D \frac{\partial^4 h}{\partial x^4} + R\theta(x, \{h\}) + \eta(x, t) \quad (1)$$

where $-D \frac{\partial^4 h}{\partial x^4}$ is the total amount of the surface diffusion current, with D being proportional to the surface diffusion; R is the deposition rate with an exposure angle of $\theta(x, \{h\})$.

Initially, the sputtering led to a decrease in the surface roughness of the silicon wafer surfaces ($R_a = 0.29$ nm), down to 0.18 nm on the 3 nm thin titanium film. As the film thickness was increased to 12 nm, the resulting surface appeared to be homogeneous, maintaining a similar topography across the surface ($R_a = 0.20$ nm) (Fig. 2). With further growth in the thickness of the titanium film to 150 nm, the surface topography further evolved to a point where it became nanoscopically rougher ($R_a = 0.52$ nm), directly as a result of the shadow effect as previously described. This implies that the positions of low height receive fewer deposited particles than those on the higher positions (such as on the peaks) due to their geometrical features. The formation of nanograins was also observed (Fig. 2). This observation is in agreement with previously reported work that describes the formation of nanograins on titanium surfaces of thicknesses between 100 nm and 300 nm³³.

Notably, with the surface structural evolution occurring as the films were grown, the R_{skw} and R_{kur} parameters did not show any significant difference (Table 1), falling quite close to 0 and 3, respectively; thus indicating that the surfaces exhibited a symmetrical distribution of bell-peaks and valleys.

The XPS analysis confirmed that in an ambient environment, titanium is present in the form of titanium dioxide (TiO_2)^{27–28}. Since the bond length in the TiO_2 molecule was estimated as being approximately 0.16 nm (Table 1, Fig. 1), which is approximately equal to the average roughness of the 3 nm and 12 nm titanium films, it can be inferred that these surfaces in particular are molecularly smooth.

During the evolution of the titanium films, the degree of surface hydrophobicity was found to be positively correlated with the degree of the surface roughness, with the roughest 150 nm film surface exhibiting the highest degree of surface hydrophobicity (displaying a contact angle of approximately 104.5°). This correlation is in accordance with the Wenzel model which explains roughness-induced hydrophobicity³⁴:

$$\cos \theta_{rough} = r \cos \theta_{smooth} \quad (2)$$

where θ_{rough} and θ_{smooth} are fluid contact angles on rough and smooth surfaces, and r is the roughness factor. If the contact angle on a smooth surface is greater than 90°, according to the Wenzel equation, it would be expected that the ‘rouger’ 150 nm titanium surface would exhibit a higher water contact angle ($\theta_w = 104.5^\circ$) than that found on the smoother 3 nm and 12 nm thin titanium film surfaces ($\theta_w = 97.4^\circ$ and 96.7° , respectively), as was the case in this study.

A summary of the bacterial attachment responses on titanium surfaces with an average surface roughness between 0.2 nm and 0.5 nm is presented in Fig. 4. A remarkably different response was observed between the *P. aeruginosa* and *S. aureus* cells. The few available accepted theories for the explanation of differential cell adhesion based on cell surface charge and hydrophobicity cannot adequately predict trends in bacterial adhesion in this case^{20,35–36}, with each of these models predicting an opposite outcome to that observed in this study. *S. aureus* is the more negatively charged bacterium of the two under investigation ($\zeta = -35.2 \pm 0.2$ mV, Supplementary Table S3), and therefore is expected to exhibit the weakest attachment propensity based on surface charge alone. On the other hand, since the surface of the *P. aeruginosa* cells exhibited a slightly more hydrophilic nature, with a water contact angle (θ) of 43°, compared to that of *S. aureus*, which exhibited less hydrophilicity ($\theta = 72^\circ$), it might be expected that the *S. aureus* cells would exhibit the stronger attachment propensity towards the highly

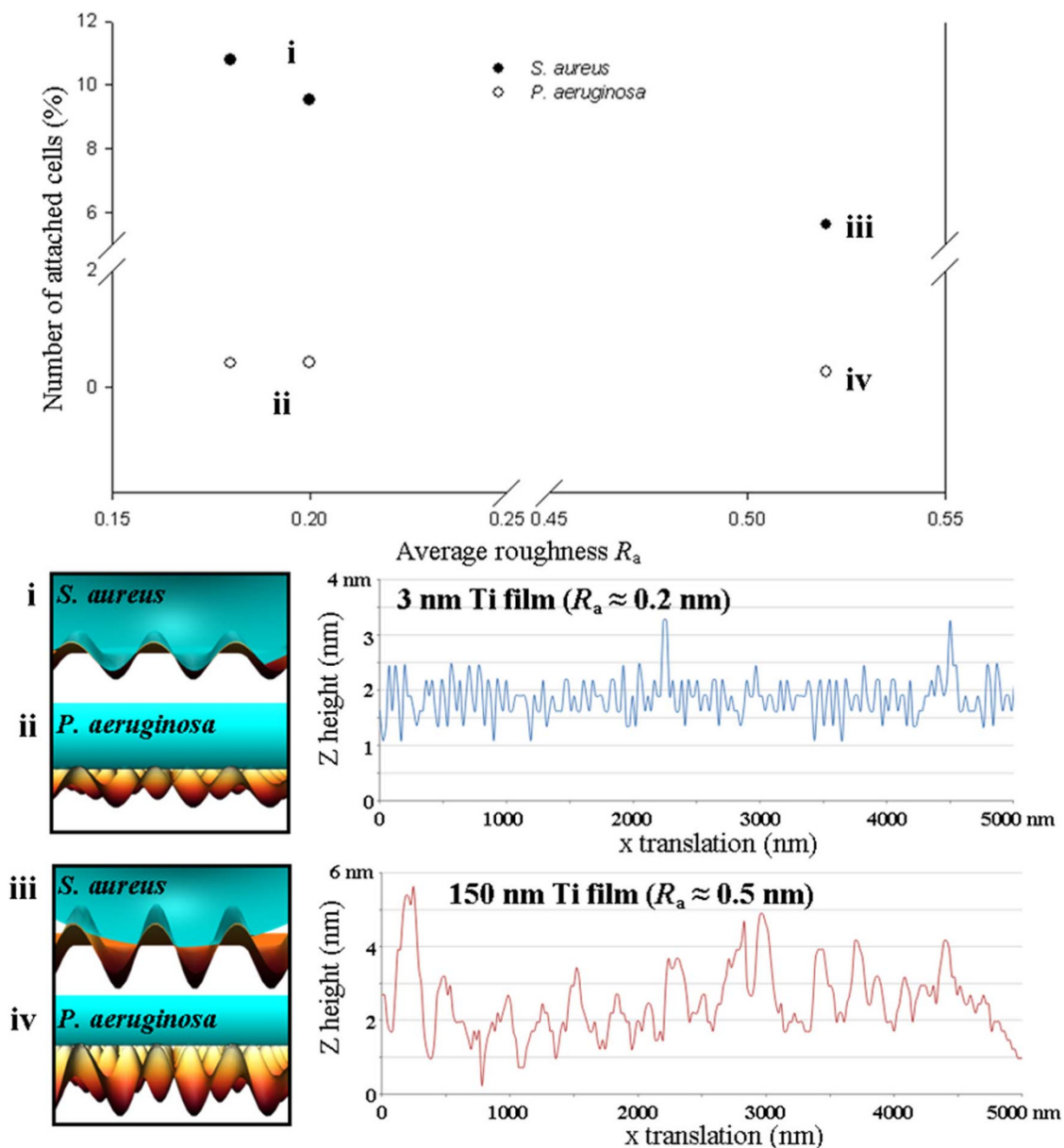


Figure 4 | Bacterial cells, *P. aeruginosa* (black circles) and *S. aureus* (white circles), attachment response on nanoscopically smooth titanium thin film surfaces (top). *S. aureus* cells attach in higher proportions on 0.2 nm roughness titanium films, due to their ability to maintain larger contact areas. This is shown in schematic diagrams of the contact regions between *S. aureus* and *P. aeruginosa* cells and model surfaces (generated using Avizo 6.3) of differing roughness (bottom left). On the rougher surface spaces remain between peaks underneath the *S. aureus* cell, while on the smoother surface contact is unbroken. The outer membrane of *P. aeruginosa* cells rests on top of the nanopoints of average roughness between 0.18 nm and 0.52 nm over $5 \mu\text{m} \times 5 \mu\text{m}$ AFM scanning areas. Peak height is exaggerated in schematics, actual surface line profiles of the 3 nm and 150 nm titanium films are provided for comparison (bottom right).

hydrophobic surfaces encountered in this study. We found that on the titanium films the attachment of *S. aureus* cells was stronger than that of *P. aeruginosa* cells. In addition, *S. aureus* cells were found to attach in greater numbers to the molecularly smooth titanium surfaces with water contact angles of 97° than those with a water contact angle of 104.5° . It is also noteworthy that the *S. aureus* cells failed to attach onto nano-scale smooth ($R_a=181$ nm) optical fiber surfaces with similar hydrophobic characteristics (water contact angle, $\theta = 106^\circ$) in a previous study¹³.

It appears that *P. aeruginosa* cell attachment is markedly restricted on titanium surfaces with an average roughness equal to or below 0.5 nm, where less than 0.5% of cells were retained on the surface. Conversely, *S. aureus* cells exhibited striking attachment persistence to attachment, especially on the 3 nm and 12 nm films, resulting in

an almost twofold increase in attached cell density compared to that observed on the 150 nm film surfaces. Taking into consideration that the physicochemical surface characteristics of titanium thin films were the same for both types of cells, it is likely that the difference in the attachment behavior originates from the differences in membrane rigidity and stretching, a property that is a function of cell morphology^{37–38}. The cellular morphology is an indirect indication of the turgor pressure inside bacterial cells which plays a contributing role in place of a cytoskeleton³⁷. Spherical cells such as *S. aureus*, have been shown to possess higher turgor pressures than rod-shaped cells, e.g., *P. aeruginosa*^{39–40}. This effect may explain the different attachment propensity of the two types of cells onto the molecularly smooth films. Low turgor pressures allow for large variability of cell shapes, since their cell membrane is relaxed and therefore has the



ability to undergo modifications in shape and fluctuate with almost no energy cost. In addition, fluctuations of a relaxed membrane near an attractive surface generate the repulsive force known as Helfrich repulsion, which is able to induce the unbinding transition⁴¹. Thermal fluctuations can be magnified by the presence of an attractive surface^{42–43}. It was recently demonstrated that monocytic cell membranes can undergo fluctuations with amplitude of 5 nm⁴⁴. Cells are able to detect the presence of foreign surfaces at a separation distance of 50 nm, and are able to establish molecular contact in the range of 30 nm–40 nm^{44–45}. In turn, high turgor pressures within a bacterial cell can cause the membrane to stretch (as described by the Laplace expression relating surface tension to pressure). As a result, the thermal fluctuations of a stretched membrane are reduced^{39,43,46}. The spherical cell geometry of *S. aureus* cells may therefore have allowed each attaching bacterium to establish a greater area of contact on the smoothest surfaces^{39,43}. Based on this hypothesis, a schematic model was constructed that demonstrated that the superior surface contact adopted by the *S. aureus* cells resulted in their ability to maintain attachment onto molecularly smooth surfaces (Fig. 4).

In summary, the data obtained in this report showed that the extent of bacterial attachment to surfaces that are molecularly smooth is different for the two types of bacterial strains used in this study. As the average surface roughness decreased from 0.52 nm to 0.18 nm, the spherical *S. aureus* cells increased in their propensity for attachment to the surface almost twofold, whereas the rod-shaped *P. aeruginosa* cells attached equally poorly to each of the molecularly smooth titanium films. We propose that the morphology of the bacterial cells (whether spherical or rod-shaped) is an indirect indication of the ability for the membrane to deform. As a result, spherical cells are less deformable and more effectively adhere to smoother surfaces. We believe that our study highlights the significance of membrane deformability of different cell morphologies on the attachment process onto molecularly smooth surfaces, where previously known mechanisms such as through interactions with the flagella and fimbriae or EPS failed to promote bacterial adhesion.

Methods

Fabrication of titanium surfaces. The titanium thin films of 3, 12 or 150 nm thickness (henceforth referred to as 3, 12 or 150 nm films) were prepared using pre-cleaned silicon wafers (<100>, NOVA Electronic Materials, Inc.) using a Kurt J Lesker CMS-18 magnetron sputtering thin film deposition system as previously described²².

Titanium thin film surface characterization. The surface compositions of the titanium-coated silicon wafers were determined from X-ray photoelectron spectra using a Kratos Axis Ultra DLD spectrometer (Kratos Analytical Ltd, U.K.), according to the previously described methodology²². The contact angles of different solvents on titanium thin films were measured using the sessile drop method⁴⁷. A scanning probe microscope (SPM) (Solver P7LS, NT-MDT) was used to obtain images of the surface morphology and to quantitatively measure and analyze the surface roughness of metallic surfaces on the nanometer scale. The analysis was performed as described elsewhere²². All samples (four for each condition) were first scanned with a 10 μm × 10 μm field of view to ensure that an even surface coverage was obtained and to avoid the presence of damaged and/or contaminated areas (data not shown), before selecting the 5 μm × 5 μm areas for scanning and analysis. All of the roughness data presented here are an average of four scans.

Statistical data processing was performed using the SPSS 18.0 program (SPSS Inc., Chicago, Illinois, USA). Paired *t*-tests were performed to evaluate the consistency of surface roughness parameters.

Interactive three-dimensional (3D) visualization of the titanium surface was undertaken with a custom C-code and the S2PLOT graphics library⁴⁸. The input data files were in NT-MDT format, and fed into the viewing tool (mdtview) using a modification of the NT-MDT module of the open software Gwyddion by David Necas and Petr Klapetek (<http://gwyddion.net/>, Version 2.12). NT-MDT files were converted into a three-dimensional surface, colored according to height, and displayed with the S2PLOT s2surpa function. Visualizations were exported from mdtview to an intermediate VRML format, with textures for axis labels in TGA format. Textures were converted to PNG format, and the VRML model was imported into Adobe Acrobat 3D Version 8 to create an interactive figure, using the approach described by Barnes and Fluke⁴⁹. JavaScript commands were used to provide additional functionality. In the on-line version of this paper, the interactive Figure S4 can be viewed by mouse clicking on the four panels, provided Adobe Reader Version 8.0

or higher is used. This opens a window where the surface can be examined interactively using the mouse to control the camera orientation and zoom level.

Computer modeling. The geometry of the singlet neutral titanium dioxide (TiO₂) in isolation was fully optimized at the hybrid density functional theory (DFT) level, using the B3LYP/cc-pVTZ model, incorporated in the GAUSSIAN09 computational chemistry package⁵⁰. Subsequent harmonic vibrational frequency analysis was used to identify the nature of optimized stationary points as real local minima (without any imaginary frequency), transition states (with only one imaginary frequency) or higher-order saddle points (with more than one imaginary frequency).

The three-dimensional model surfaces were constructed by generating two-dimensional height data using Microsoft Excel and Avizo Software, version 6.3.

Bacterial Growth and Sample Preparation. Two bacterial strains, *Staphylococcus aureus* CIP 65.8 and *Pseudomonas aeruginosa* ATCC 9027, were used. Bacterial strains were obtained from the American Type Culture Collection (ATCC, USA) and the Culture Collection of the Institute Pasteur (CIP, France). Bacterial strain stocks were prepared in 20% glycerol nutrient broth (Merck) and stored at –80 °C. Both strains were cultured on nutrient agar (Oxoid) and nutrient broth (Oxoid) at room temperature (ca. 22 °C). In addition, incubation at 37 °C was also tested to confirm whether the bacterial attachment pattern will be affected. No statistically significant differences were found (data not shown).

Prior to each experiment, a fresh bacterial suspension was prepared as previously reported²². At least two independent experiments in triplicate and with correspondent controls have been performed.

Visualization and Quantification of Viable Cells and EPS. In order to visualize viable bacteria and the EPS, standard staining techniques were used. The bacteria were stained with SYTO[®] 17 Red (Molecular Probes[™], Invitrogen) and the EPS was stained green with Alexa Fluor[®] 488 (Molecular Probes[™], Invitrogen), a conjugate of succinylated concanavalin A²². Images of the bacteria attached to titanium surfaces and the EPS were recorded with a confocal laser scanning microscope (CSLM) Olympus Fluorview FV1000 Spectroscopic Confocal System. The system included an inverted microscope OLYMPUS IX81 [with 20×, 40× (oil), 100× (oil) UIS objective lenses] and was operated with multiple Ar, He and Ne laser lines (458, 488, 515, 543, 633 nm). The 488 nm laser was used to image the concanavalin A Alexa[®] 488 dye and the 543 nm laser was used to image the SYTO[®] 17 Red. Avizo package, version 6.3 was employed to process the CSLM images and construct 3D visualization.

To quantify 3D biofilm image stacks, specialized computer software, COMSTAT, was used⁵¹. Scanned areas were exported into a stack of grey-scale 8-bit images by Fluoview FV 7.0. Two quantitative parameters of biomass density were used to describe the pattern of attached bacterial cells on the titanium surfaces⁵¹: (i) the biovolume, which encompasses both cells and EPS, and (ii) the average biofilm thickness. Both parameters have the dimension of length: the biovolume represents the overall volume of the cells and EPS per unit area of substrate and the average biofilm thickness provides a measure of depth size of the cells and EPS. For the purposes of statistical analysis twenty five fields of view were examined.

In all scanning electron microscopy experiments, titanium surfaces with attached bacteria were gold-coated as previously reported²². High-resolution images of titanium thin films with the retained bacterial cells were taken using an FESEM (ZEISS SUPRA 40VP) at 3 kV at 1,000×, 5,000× and 20,000× magnification. Images at 1,000× and 5,000× magnification were used to calculate the number of bacteria attaching to the titanium surfaces; the results were statistically analyzed. Each of attachment experiments were repeated twice and five data points of each repeat were collected.

1. Ploux, L. *et al.* Opposite responses of cells and bacteria to micro/nanopatterned surfaces prepared by pulsed plasma polymerization and UV-irradiation. *Langmuir* **25**, 8161–8169 (2009).
2. Truong, V. K. *et al.* Effect of ultrafine-grained titanium surfaces on adhesion of bacteria. *Appl Microbiol Biotech* **83**, 925–937 (2009).
3. Gentile, F. *et al.* Cells preferentially grow on rough substrates. *Biomaterials* **31**, 7205–7212 (2010).
4. Puckett, S. D., Taylor, E., Raimondo, T. & Webster, T. J. The relationship between the nanostructure of titanium surfaces and bacterial attachment. *Biomaterials* **31**, 706–713 (2010).
5. Hochbaum, A. I. & Aizenberg, J. Bacteria pattern spontaneously on periodic nanostructure arrays. *Nano Letters* **10**, 3717–3721 (2010).
6. Ivanova, E. P., Pham, D. K., Wright, J. P. & Nicolau, D. V. Detection of coccoid forms of *Sulfitobacter mediterraneus* using atomic force microscopy. *FEMS Microbiology Letters* **214**, 177–181 (2002).
7. Rowan, B., Wheeler, M. A. & Crooks, R. M. Patterning bacteria within hyperbranched polymer film templates. *Langmuir* **18**, 9914–9917 (2002).
8. Rozhok, S. *et al.* Attachment of motile bacterial cells to prealigned holed microarrays. *Langmuir* **22**, 11251–11254 (2006).
9. Ivanova, E. P. *et al.* *Staleyia guttififormis* attachment on poly(tert-butylmethacrylate) polymeric surfaces. *Micron* **39**, 1197–1204 (2008).
10. Mitik-Dineva, N. *et al.* Impact of nano-topography on bacterial attachment. *Biotechnology Journal* **3**, 536–544 (2008).



11. Webb, H. K., Crawford, R. J., Sawabe, T. & Ivanova, E. P. Poly(ethylene terephthalate) polymer surfaces as a substrate for bacterial attachment and biofilm formation. *Microbes and Environments* **24**, 39–42 (2009).
12. Mitik-Dineva, N. *et al.* Differences in colonisation of five marine bacteria on two types of glass surfaces. *Biofouling* **25**, 621–631 (2009).
13. Mitik-Dineva, N. *et al.* Bacterial attachment on optical fibre surfaces. *Biofouling* **26**, 461–470 (2010).
14. Díaz, C., Schilardi, P. L., Salvarezza, R. C. & Fernández Lorenzo de Mele, M. Nano/Microscale Order Affects the Early Stages of Biofilm Formation on Metal Surfaces. *Langmuir* **23**, 11206–11210 (2007).
15. Mitik-Dineva, N. *et al.* *Escherichia coli*, *Pseudomonas aeruginosa* and *Staphylococcus aureus* Attachment Patterns on Glass Surfaces with Nanoscale Roughness. *Current Microbiology* **58**, 268–273 (2009).
16. Whitehead, K. A., Colligon, J. & Verran, J. Retention of microbial cells in substratum surface features of micrometer and sub-micrometer dimensions. *Colloids Surf. B Biointerfaces* **41**, 129–138 (2005).
17. An, Y. H. *et al.* Rapid quantification of *Staphylococci* adhered to titanium surfaces using image analyzed epifluorescence microscopy. *Journal of Microbiological Methods* **24**, 29–40 (1995).
18. Boulangé-Petermann, L., Rault, J. & Bellon-Fontaine, M. N. Adhesion of *Streptococcus thermophilus* to stainless steel with different surface topography and roughness. *Biofouling* **11**, 201–216 (1997).
19. Medilanski, E., Kaufmann, K., Wick, L. Y., Wanner, O. & Harms, H. Influence of the surface topography of stainless steel on bacterial adhesion. *Biofouling* **18**, 193–203 (2002).
20. Li, B. & Logan, B. E. Bacterial adhesion to glass and metal-oxide surfaces. *Colloids and Surfaces B: Biointerfaces* **36**, 81–90 (2004).
21. Whitehead, K. A., Rogers, D., Colligon, J., Wright, C. & Verran, J. Use of the atomic force microscope to determine the effect of substratum surface topography on the ease of bacterial removal. *Colloids Surf. B Biointerfaces* **51**, 44–53 (2006).
22. Ivanova, E. P. *et al.* Impact of Nanoscale Roughness of Titanium thin films surfaces on Bacterial Retention. *Langmuir* **26**, 1973–1982 (2010).
23. Truong, V. K. *et al.* The influence of nanoscale surface roughness on bacterial adhesion to ultrafine-grained titanium. *Biomaterials* **31**, 3674–3683 (2010).
24. Wang, J. Y., Ghantasala, M. K. & McLean, R. J. Bias sputtering effect on ultra-thin SmCo5 films exhibiting large perpendicular coercivity. *Thin Solid Films* **517**, 656–660 (2008).
25. Jeyachandran, Y. L. *et al.* Properties of titanium thin films deposited by dc magnetron sputtering. *Materials Science and Engineering A* **431**, 277–284 (2006).
26. McCafferty, E. & Wightman, J. P. X-ray photoelectron spectroscopy sputter profile study of the native air-formed oxide film on titanium. *Applied Surface Science* **143**, 92–100 (1999).
27. Bertóti, I., Mohai, M., Sullivan, J. L. & Saied, S. O. Surface characterisation of plasma-nitrided titanium: an XPS study. *Applied Surface Science* **84**, 357–371 (1995).
28. Cai, K., Muller, M., Bossert, J., Rechtenbach, A. & Jandt, K. Surface structure and composition of flat titanium thin films as a function of film thickness and evaporation rate. *Appl Surf Sci* **250**, 252–267 (2005).
29. Qu, Z. W. & Kroes, G. J. Theoretical study of the electronic structure and stability of titanium dioxide clusters (TiO₂)_n with n = 1–9. *Journal of Physical Chemistry B* **110**, 8998–9007 (2006).
30. McIntyre, N. S., Thompson, K. R. & Weltner Jr, W. Spectroscopy of titanium oxide and titanium dioxide molecules in inert matrices at 4°K. *Journal of Physical Chemistry* **75**, 3243–3249 (1971).
31. Gadelmawla, E. S., Koura, M. M., Maksoud, T. M. A., Elewa, I. M. & Soliman, H. H. Roughness parameters. *J Mater Process Technol* **123**, 133–145 (2002).
32. Lamolle, S. F. *et al.* The effect of hydrofluoric acid treatment of titanium surface on nanostructural and chemical changes and the growth of MC3T3-E1 cells. *Biomaterials* **30**, 736–742 (2009).
33. Karunasiri, R. P. U., Bruinsma, R. & Rudnick, J. Thin-film growth and the shadow instability. *Phys Rev Lett* **62**, 788–791 (1989).
34. Wenzel, R. N. Surface roughness and contact angle. *Journal of Physical & Colloid Chemistry* **53**, 1466–1467 (1949).
35. Bayouhd, S. *et al.* Quantification of the adhesion free energy between bacteria and hydrophobic and hydrophilic substrata. *Mater. Sci. Eng. C* **26**, 300–305 (2006).
36. Bruinsma, G. M., Van Der Mei, H. C. & Busscher, H. J. Bacterial adhesion to surface hydrophilic and hydrophobic contact lenses. *Biomaterials* **22**, 3217–3224 (2001).
37. Koch, A. L. Bacterial wall as target for attack: Past, present, and future research. *Clin. Microbiol. Rev.* **16**, 673–687 (2003).
38. Harold, F. M. Bacterial morphogenesis: learning how cells make cells. *Curr. Opin. Microbiol.* **10**, 591–595 (2007).
39. Whatmore, A. M. & Reed, R. H. Determination of Turgor Pressure in *Bacillus subtilis*: A Possible Role for K⁺ in Turgor Regulation. *J. Gen. Microbiol.* **136**, 2521–2526 (1990).
40. Arnoldi, M. *et al.* Bacterial turgor pressure can be measured by atomic force microscopy. *Phys. Rev. E* **62**, 1034–1044 (2000).
41. Netz, R. R. Complete Unbinding of Fluid Membranes in the Presence of Short-Range Forces. *Phys. Rev. E* **51**, 2286–2294 (1995).
42. Prost, J., Manneville, J. B. & Bruinsma, R. Fluctuation-magnification of non-equilibrium membranes near a wall. *Eur. Phys. J. B* **1**, 465–480 (1998).
43. Marrink, S. J. & Mark, A. E. Effect of undulations on surface tension in simulated bilayers. *Journal of Physical Chemistry B* **105**, 6122–6127 (2001).
44. Pierres, A., Benoliel, A. M., Touchard, D. & Bongrand, P. How cells tiptoe on adhesive surfaces before sticking. *Biophysical Journal* **94**, 4114–4122 (2008).
45. Pierres, A., Monnet-Corti, V., Benoliel, A. M. & Bongrand, P. Do membrane undulations help cells probe the world? *Trends Cell Biol.* **19**, 428–433 (2009).
46. Cretel, E., Pierres, A., Benoliel, A. M. & Bongrand, P. How Cells Feel Their Environment: A Focus on Early Dynamic Events. *Cell. Mol. Bioeng.* **1**, 5–14 (2008).
47. Öner, D. & McCarthy, T. J. Ultrahydrophobic surfaces. Effects of topography length scales on wettability. *Langmuir* **16**, 7777–7782 (2000).
48. Barnes, D., Fluke, C., Bourke, P. & Parry, O. An advanced, three-dimensional plotting library for astronomy. *Publications of the Astronomical Society of Australia* **23**, 82–93 (2006).
49. Barnes, D. & Fluke, C. Incorporating interactive three-dimensional graphics in astronomy research papers. *New Astronomy* **13**, 599–605 (2008).
50. GAUSSIAN09 (Washington, CT., 2009).
51. Heydorn, A. *et al.* Quantification of biofilm structures by the novel computer program COMSTAT. *Microbiology* **146**, 2395–2407 (2000).

Acknowledgements

This study was supported in part by Advanced Manufacturing Co-operative Research Centre (AMCRC). V.K.T., H.K.W. and N.M. are recipients of Swinburne University Postgraduate Research Awards (SUPRA).

Author contributions

E.P.I. designed the study, analyzed data, wrote the paper; V.K.T. performed surface characterization, collected data on bacterial attachment experiments, and helped write the paper; H.K.W. prepared figures 2–4, helped write the paper; V.B. was involved in the study design; J.W. was involved in sample fabrication, AFM and SEM data analysis; C.F. was involved in AFM data analysis contributing in Figure 2 preparation; N.M. and F.W. performed computer modeling; R.J.C. was involved in the study design, data analysis, and helped write the paper. All the authors discussed the results, commented on the manuscript, and approved the manuscript.

Additional information

Supplementary information accompanies this paper at <http://www.nature.com/scientificreports>

Competing financial interests: The authors declare no competing financial interests.

License: This work is licensed under a Creative Commons Attribution-NonCommercial-ShareAlike 3.0 Unported License. To view a copy of this license, visit <http://creativecommons.org/licenses/by-nc-sa/3.0/>

How to cite this article: Ivanova, E.P. *et al.* Differential attraction and repulsion of *Staphylococcus aureus* and *Pseudomonas aeruginosa* on molecularly smooth titanium films. *Sci. Rep.* **1**, 165; DOI:10.1038/srep00165 (2011).